Article

Cell Reports

Timed Synaptic Inhibition Shapes NMDA Spikes, Influencing Local Dendritic Processing and Global I/O Properties of Cortical Neurons

Graphical Abstract

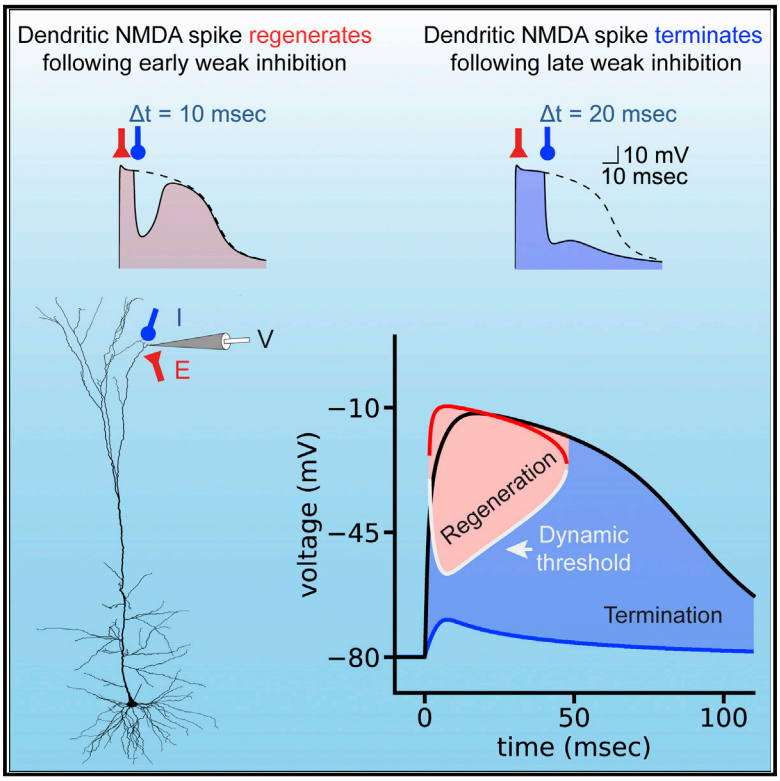

Authors

Michael Doron, Giuseppe Chindemi, Eilif Muller, Henry Markram, Idan Segev

Correspondence

michael.doron@mail.huji.ac.il

In Brief

The NMDA spike is a nonlinear dendritic phenomenon involved in synaptic plasticity and in shaping the I/O properties of neurons. Doron et al. use a theoretical approach to study the fine-tuned and powerful modulation of the NMDA spike by timed synaptic inhibition. They provide a mechanistic explanation for the interaction between timed inhibition and excitation and explore the implications for dendritic and somatic computations.

Highlights

- Local dendritic NMDA spike is finely modulated by timed, branch-specific inhibition
- Dynamic system analysis explains the vulnerability of the NMDA spike to inhibition
- Dendritic, but not spine, inhibition strongly shapes the NMDA-spike-mediated Ca^{2+} current
- Sparse, weak distal inhibition finely sculpts NMDA-mediated output spike bursts

Doron et al., 2017, Cell Reports *21*, 1550–1561
November 7, 2017
https://doi.org/10.1016/j.celrep.2017.10.035

OPEN ACCESS
CellPress

Cell Reports
Article

Timed Synaptic Inhibition Shapes NMDA Spikes, Influencing Local Dendritic Processing and Global I/O Properties of Cortical Neurons

Michael Doron,[1,4,*] Giuseppe Chindemi,[2] Eilif Muller,[2] Henry Markram,[2] and Idan Segev[1,3]
[1]Edmond and Lily Safra Center for Brain Sciences, the Hebrew University of Jerusalem, Jerusalem 91904, Israel
[2]Blue Brain Project, École polytechnique fédérale de Lausanne (EPFL), Biotech Campus, 1202 Geneva, Switzerland
[3]Department of Neurobiology, the Hebrew University of Jerusalem, Jerusalem 91904, Israel
[4]Lead Contact
*Correspondence: michael.doron@mail.huji.ac.il
https://doi.org/10.1016/j.celrep.2017.10.035

SUMMARY

The NMDA spike is a long-lasting nonlinear phenomenon initiated locally in the dendritic branches of a variety of cortical neurons. It plays a key role in synaptic plasticity and in single-neuron computations. Combining dynamic system theory and computational approaches, we now explore how the timing of synaptic inhibition affects the NMDA spike and its associated membrane current. When impinging on its early phase, individual inhibitory synapses strongly, but transiently, dampen the NMDA spike; later inhibition prematurely terminates it. A single inhibitory synapse reduces the NMDA-mediated Ca^{2+} current, a key player in plasticity, by up to 45%. NMDA spikes in distal dendritic branches/spines are longer-lasting and more resilient to inhibition, enhancing synaptic plasticity at these branches. We conclude that NMDA spikes are highly sensitive to dendritic inhibition; sparse weak inhibition can finely tune synaptic plasticity both locally at the dendritic branch level and globally at the level of the neuron's output.

INTRODUCTION

The possibility that the nonlinear properties of the dendritic membrane might endow dendrites with enhanced computational and plastic capabilities was first suggested more than 50 years ago by Rall and Shepherd (1968), Rall et al. (1966), and Segev and Rall (1988) and, more recently, by Mel (1992, 1993), Poirazi and Mel (2001), and Poirazi et al. (2003a). Advances in molecular and optical techniques have demonstrated that dendrites are rich in a myriad of nonlinear membrane ion channels (Johnston and Narayanan, 2008; Magee, 2016) and that these channels are involved in specific plastic, computational, and cognitive processes (Cuntz et al., 2014; Hoffman et al., 1997; Poirazi et al., 2003b). In that respect, of particular interest are the recently discovered Na^+, Ca^{2+}, and NMDA dendritic spikes (Golding et al., 2002; Larkum et al., 1999; Schiller et al., 2000). The latter NMDA spike was shown to be generated locally in multiple apical and basal dendritic branches of both cortical and hippocampal pyramidal neurons (Branco and Häusser, 2011; Lavzin et al., 2012; Major et al., 2013; Miloj-kovic et al., 2004; Nevian et al., 2007; Poleg-Polsky, 2015; Schiller et al., 2000). It has been shown that dendritic Na^+, Ca^{2+}, and NMDA spikes can implement a variety of computational functions, including input pattern classification (Mel, 1992), coincidence detection (Larkum and Nevian, 2008; Schiller and Schiller, 2001), and directional selectivity (Branco et al., 2011; Smith et al., 2013). Importantly, the Ca^{2+} influx associated with dendritic spikes plays a key role in modulating the plasticity of dendritic synapses (Gambino et al., 2014; Gordon et al., 2006; Sandler et al., 2016; Villa et al., 2016).

Nonlinear dendritic signals could be effectively modulated by dendritic inhibition. Theoretical studies have shown that a well-located dendritic inhibition, when preceding its respective dendritic/somatic spikes, could either completely abolish these spikes or modulate their amplitude (Gidon and Segev, 2012; Jadi et al., 2012; Rhodes, 2006). It was recently demonstrated that NMDA spikes, and their resultant somatic bursts of Na^+ spikes, are regulated by SOM^+ interneurons (Lovett-Barron et al., 2012). Müllner et al. (2015) show that a single GABAergic contact can strongly, and locally, reduce the influx of Ca^{2+} current originating from the backpropagating action potential. These studies show that sparse dendritic inhibition can effectively modulate dendritic excitability and its associated plasticity-inducing signals. It is worth noting in this context that, in both the cerebral cortex and the hippocampus, different classes of inhibitory interneurons target pyramidal neuron dendrites in different dendritic domains (Klausberger, 2009; Markram et al., 2004; Stokes et al., 2014) and are activated in different behavioral states (e.g., sleep cycles). This raises the interesting possibility that the various types of interneurons might selectively control different nonlinear dendritic signals. For instance, Martinotti cells that mostly target the distal apical tree might selectively control NMDA spikes in distal apical dendrites; basket inhibition might selectively control the Ca^{2+} generated at the main apical branch of layer 5 (L5) and L2/3 pyramidal cells; and chandelier inhibition (targeting the initial segment of the axon of pyramidal neurons) could selectively control the somatic/axonal Na^+ spike (Gidon and Segev, 2012).

Yet little is known about how synaptic inhibition interacts with the NMDA spike after it has been initiated. Because the NMDA spike is long-lasting (Major et al., 2008), it is likely that synaptic

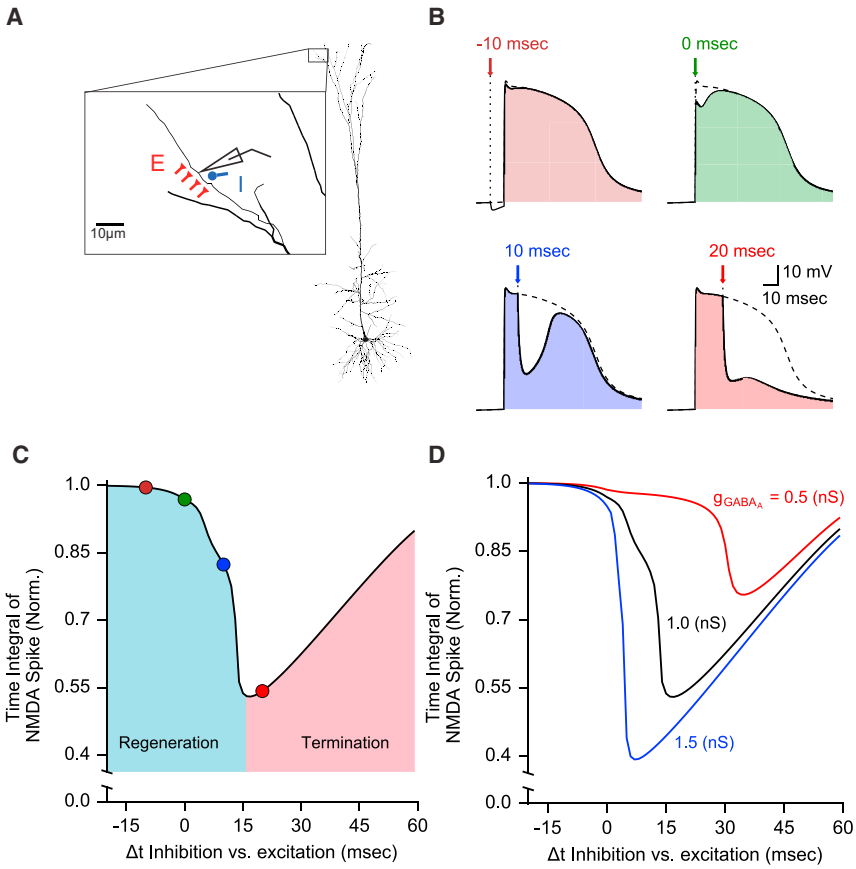

Figure 1. Dendritic NMDA Spikes Are Susceptible to Timed Synaptic Inhibition

(A) Reconstructed L5 pyramidal neuron model. Twenty synchronously activated AMPA- and NMDA-based excitatory synapses (red) and a single $GABA_A$ synapse (blue) were distributed around the center of a distal apical dendritic branch from which the membrane voltage was recorded (schematic electrode).

(B) NMDA spikes generated in the modeled dendritic branch shown in (A); arrows point to the inhibition activation time. NMDA spike in the presence of inhibition (colored area); dashed trace without inhibition.

(C) Normalized time integral of the NMDA spike for different activation times of the inhibitory synapse (the "vulnerability function"). Colored dots on the black curve correspond to the respective traces in (B). The blue and red areas, respectively, denote the regeneration and termination phases of the NMDA spike.

(D) As in (C), with different $GABA_A$ peak conductance values.

activity *in vivo* will bombard the NMDA during its plateau phase particularly because *in vivo* inhibition is activated at a relatively high frequency and is often activated following excitation (Ma et al., 2010; Pouille and Scanziani, 2001; Silberberg and Markram, 2007; Wehr and Zador, 2003). How would the NMDA spike react to such timed inhibition? Would it be completely abolished, or would the NMDA spike, and its associated current influx, be finely tuned by such inhibition? We explored these questions by using various models of the NMDA spike, realistic dendritic morphology, and the properties of inhibitory synapses. We applied dynamic system theory combined with computer simulations to explore how inhibition interacts with and affects the dynamics of the NMDA spike. Our results suggest that because of the slow kinetics and unique membrane mechanisms underlying the NMDA spike, it could be sensitively modulated by well-timed local dendritic inhibition. This inhibition may gradually tune both the spiking output of the neuron and the plasticity of synapses at the level of individual dendritic branches and their respective dendritic spines.

RESULTS

Sculpting the NMDA-Spike Voltage Trajectory by Timed Synaptic Inhibition

Figure 1 illustrates the strong impact that timed weak dendritic inhibition can have on the NMDA spike. The modeled NMDA spike was initiated by simultaneously activating 20 excitatory AMPA- and NMDA-based synapses (0.4 nS peak conductance each) impinging on a distal apical branch of a 3D-reconstructed L5 neocortical pyramidal cell. A single $GABA_A$-mediated inhibitory synapse (1 nS peak conductance) located in the center of the excitatory synapses was activated at various times relative to the excitatory synapses. As expected, this rather small inhibitory conductance had a very small effect on the voltage trajectory of the NMDA spike when it preceded excitation. The same weak inhibition generated stronger hyperpolarization when activated at the plateau phase of the NMDA spike, at a delay of Δt = 10 ms after excitation. Surprisingly, the NMDA spike fully recovered to its original trajectory from this hyperpolarization (Figure 1B, blue trace). When inhibition was further delayed (Δt = 20 ms), the NMDA spike was prematurely terminated (Figure 1B, lower right), and the voltage continued to hyperpolarize after the inhibitory input.

To quantify this sensitivity of the NMDA spike to timed inhibition riding on its plateau potential, we plotted the time integrals of the NMDA spike normalized to control conditions (without inhibition, dashed traces in Figure 1B) as a function of Δt (Figure 1C). We term this the "vulnerability function" of the NMDA spike to inhibition. The effect of inhibition during the time course of the NMDA spike could be divided into two distinct regimes, which we call the "regeneration" and "termination" phases. In the "regeneration" phase, the NMDA plateau hyperpolarizes because of the inhibition and then fully recovers to its original trajectory at the cessation of inhibition (light blue region in Figure 1C). In this regenerative phase, the time integral of the NMDA spike voltage dropped continuously to up to ~55% of its original time integral (at about Δt = 15 ms, Figure 1). For later Δt values, the

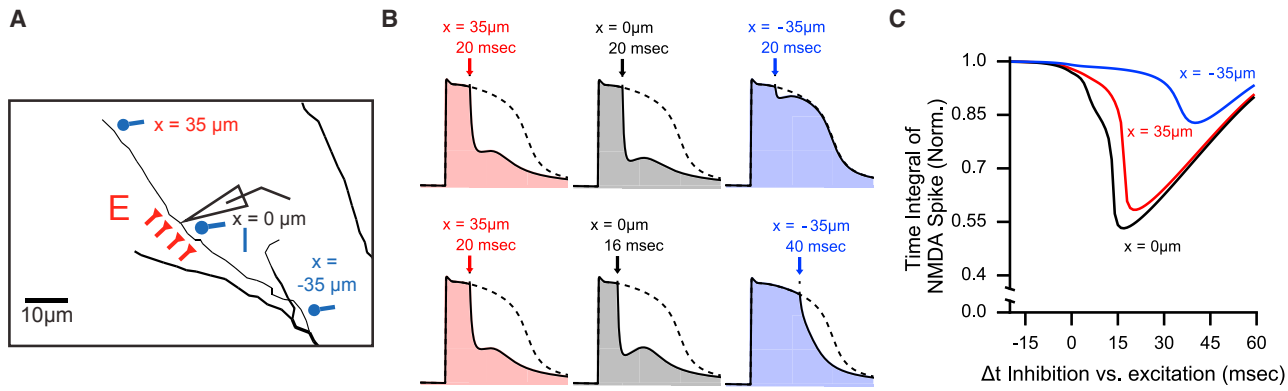

Figure 2. NMDA Spikes Are Affected More by Distal Inhibition Than by Proximal Inhibition

(A) Like in Figure 1A, with three locations, x, of the inhibitory synapse with respect to the excitatory synapses.

(B) (Top) As in Figure 1B, with inhibition arriving at Δt = 20 ms. Each trace shows the NMDA spike for the three inhibitory locations as in (A); "on spot" inhibition (x = 0, black) and distal inhibition (x = 35 μm, red) are almost as effective in dampening the NMDA spike, whereas proximal inhibition (x = −35 μm, blue) has a much smaller effect on the NMDA spike. (Bottom) Same as top, with inhibition arriving at each location at the time when it reduced the NMDA maximally.

(C) Vulnerability function for different dendritic locations.

NMDA spike was prematurely terminated by the inhibition (red region in Figure 1C, Δt = 20 ms in Figure 1B). After the NMDA spike entered the "termination" phase, its time integral increased almost linearly with progressively later inhibition. For larger GABAergic conductance, the termination phase started earlier and the time integral of the NMDA spike was further reduced by inhibition (Figure 1D). This two-regime sensitivity of the NMDA spike to timed inhibition was robust across different parameter ranges and across different models of the NMDA receptor current (Figure S1).

Distal Dendritic Inhibition Is Particularly Effective in Modulating the NMDA Spike

Next, we examined how the location and activation timing of the inhibitory synapse affect the NMDA spike. As in Figure 1A, the NMDA synapses were placed in the center of the dendritic branch, but the location of the inhibitory $GABA_A$ synapse was shifted with respect to the location of the excitatory synapses (Figure 2A). The inhibitory synapse was placed either at 35 μm distal to the center of the dendritic branch, in its center, or 35 μm proximal to it (Figure 2A). The weak inhibitory synapse, when located more distal to the soma relative to the NMDA synapses and activated at Δt = 20 ms, terminated the NMDA spike (red NMDA spike in Figure 2B); inhibition more proximal to the soma hardly affected the NMDA spike (blue NMDA spike in Figure 2B). Furthermore, the timing of the inhibition that maximally affected the time integral of the NMDA spike was earlier for the distal synapse and later (and less effective) for the proximal synapse (Figure 2B, bottom). The vulnerability function deepened significantly when the inhibitory synapse was located either directly at x = 0 or distally to the NMDA synapses, at x = 35 μm (Figure 2C). This finding is consistent with the results of Gidon and Segev (2012), who studied the impact of dendritic inhibition on the more global dendritic Ca^{2+} spike generated at the main branch of the apical dendrite (see also Figure S7).

Dynamic Analysis of the Biphasic Effect of Inhibition on the NMDA Spike

We studied the behavior of the voltage-current (V-I) relationship of the NMDA spike in the presence of synaptic inhibition as a dynamical system, using a single compartment neuron model consisting of leak ion channels and AMPA-, NMDA-, and $GABA_A$-based synapses. As was shown by Jadi et al. (2012) and Sanders et al. (2013), the NMDA current, when accompanied by the leak current, creates a bistable dynamical system with three fixed points (Figure 3A). At these fixed points, the net membrane current is zero. By perturbing the voltage around the fixed points, the leftmost intersection ("lower stable" in Figure 3A) emerges as a stable fixed point, because a small hyperpolarization from this point will produce an inward current that will result in depolarization back to the fixed point, whereas a small depolarization will produce an outward current that will result in hyperpolarization back to the fixed point (arrows around the blue circle, Figure 3A). Similarly, the rightmost intersection ("upper stable" in Figure 3A) is also a stable fixed point. The middle intersection, however, is an unstable fixed point; a small depolarization will produce an inward current that will further depolarize the membrane and a small hyperpolarization from this point will produce an outward current that will result in further hyperpolarization. This point was thus dubbed the "unstable threshold"; i.e., the critical voltage beyond which, due to depolarization, the membrane voltage will change regeneratively, thus initiating the NMDA spike (Jack et al., 1975, Figure 8.11; see also, e.g., Major et al., 2013).

Because the inward NMDA current changes over time, the fixed points also change over time (Figure 3B). We define the "regenerative" region of the NMDA spike as the regime whereby, following small voltage perturbations (that remain above the middle fixed point), the voltage will converge to the upper fixed point (shaded light red region in Figure 3B). The complementary shaded blue region in Figure 3B was termed the "termination" region of the NMDA spike because a small perturbation of the

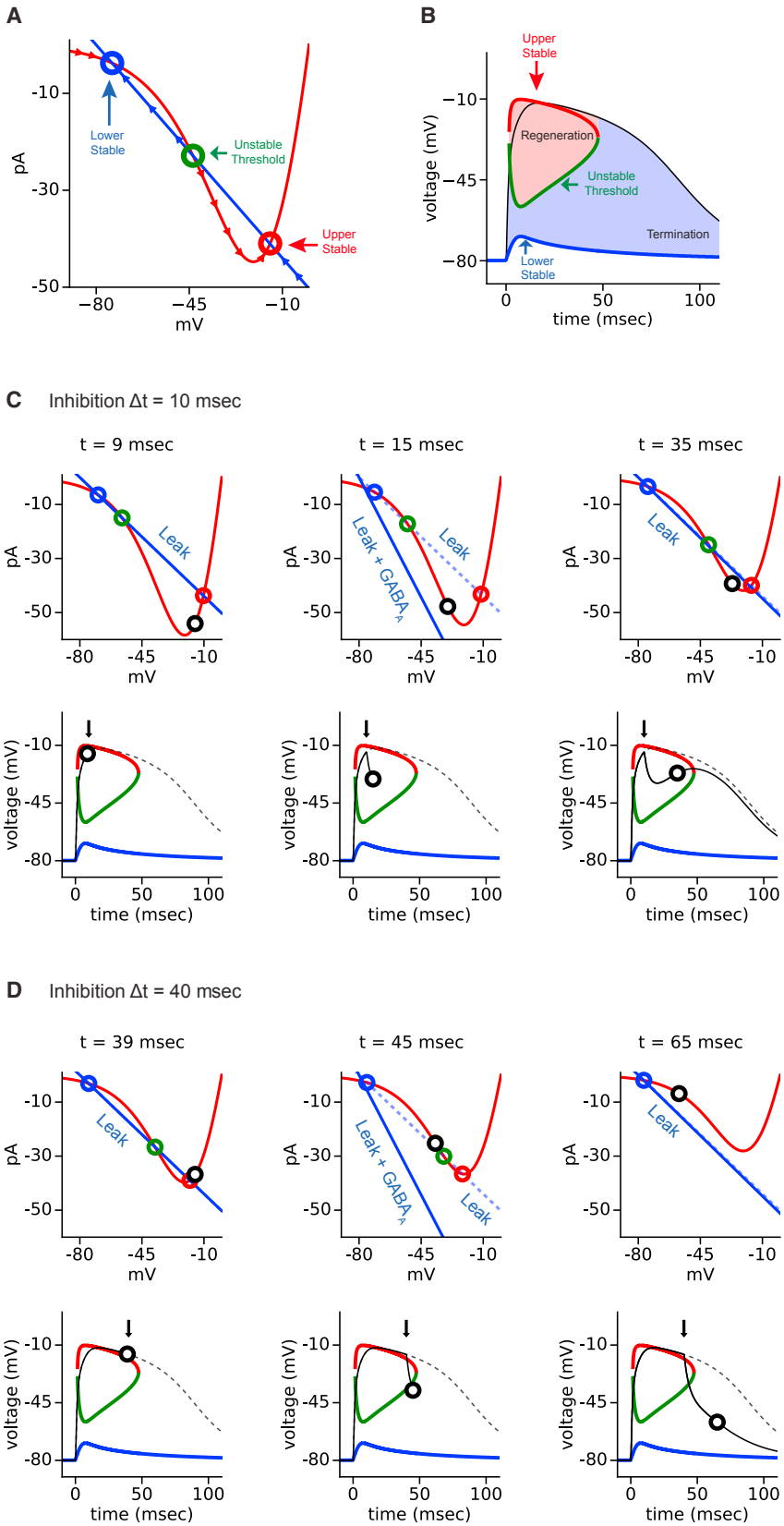

Figure 3. Mechanistic Explanation of the Dynamic Vulnerability of the NMDA Spike to Timed Inhibition

(A) The momentary voltage-current (V-I) curve for the NMDA current (red trace) and the leak current (with reversed sign, blue line) in an isopotential neuron model. These currents were measured at Δt = 30 ms following the onset of synaptic excitation (see the Experimental Procedures). The intersections between these two curves (colored circles) constitute three fixed points. Arrows on the red and blue curves indicate the direction of the voltage at that time point following a small perturbation around these fixed points.

(B) The trajectory of the three fixed points over the time course of the NMDA receptor activation (red, green, and blue like in A), plotted together with the voltage trajectory of the NMDA spike (black). The "regeneration" area is colored in red and the "termination" area in blue.

(C) Inhibition (at Δt = 10 ms) during the early phase of the NMDA spike hyperpolarized the voltage, but it remained in the regeneration regime, allowing the NMDA spike to fully recover following inhibition. (Top) As in (A) for the three time points. Blue lines depict the leak and the $GABA_A$ current (reversed in sign) at the respective times. The black circle represents the membrane voltage at these time points. (Bottom) As in (B). The NMDA spike without inhibition is shown by the dashed line; the voltage trace of the NMDA spike with inhibition up to the respective time point is shown by the solid black line in the left and middle frames. The black circle represents the voltage at the respective time points. The black arrow marks the time of activation of the inhibitory synapse (Δt = 10 ms). The solid black line in the rightmost frame shows the whole voltage trajectory of the NMDA spike following the inhibition.

(D) Similar to (C), with inhibition arriving at Δt = 40 ms. In this case inhibition hyperpolarized the NMDA spike to below threshold, terminating the NMDA spike.

voltage inside this region will result in further hyperpolarization toward the lower fixed point. Examination of the trajectories of the fixed points shows that during the time course of the NMDA spike, the threshold (the green curve in Figure 3B) is relatively hyperpolarized in the early stages and progressively becomes more depolarized with time. This accounts for the recovery of the NMDA spike in the case of early inhibition and the premature termination of the NMDA spike following later inhibition, since inhibition-induced hyperpolarization that does not cross the threshold in its early hyperpolarized state may still cross the threshold when arriving later in its depolarized state.

This behavior is depicted in more detail in Figure 3C, which illustrates the case of early inhibition arriving at Δt = 10 ms following the initiation of the NMDA spike. The three momentary V-I curves (top) and the respective voltage trajectories (bottom) were sampled at t = 9, 15, and 35 ms during the NMDA spike. At t = 9 ms (before inhibition was activated), the NMDA spike was in the regeneration region and was still depolarizing. Following the activation of inhibition, the $GABA_A$ current was added to the outward leak current, thus shifting the dashed blue curve (the leak current) to the steeper solid blue line (Figure 3C, top middle frame). At t = 15 ms, the additional inhibitory current gave rise to only a single hyperpolarized intersection point with the red V-I curves resulting in further hyperpolarization of the NMDA spike (Figure 3C, bottom middle frame). This inhibitory current continued to hyperpolarize the NMDA spike transiently, until the $GABA_A$ current ended. At later times (e.g., t = 35 ms), the outward current converged back to the leak current (solid and dashed blue lines are superimposed in Figure 3C, top right). In this case, the early inhibition hyperpolarized the NMDA spike voltage to −30 mV (black circle in Figure 3C, middle frames), which was still more depolarized than the threshold (green line in Figure 3C, bottom frames). Consequently, the voltage remained in the "regeneration" region, allowing the NMDA spike to recover back to the upper stable fixed point (Figure 3C, bottom right).

In contrast, when the inhibition arrived later, at Δt = 40 ms (Figure 3D), the NMDA spike threshold was more depolarized. In this case, the hyperpolarization due to inhibition crossed the threshold for the NMDA spike (green circle in middle top and green curve in bottom middle of Figure 3D, respectively). The voltage perturbation due to inhibition resided in the "termination" region that further hyperpolarized the NMDA spike until its premature termination.

Branch-Specific NMDA-Spike "Vulnerability Function"

Figure 4 shows that for a fixed NMDA conductance, the NMDA spikes in dendritic branches with large input resistance were longer-lasting and more resilient to $GABA_A$ inhibition as compared to branches with small input resistance. In Figure 4A, a long-lasting (61 ms) NMDA spike was generated in a distal apical branch with large input resistance (1,285 MΩ), whereas a briefer (25 ms) spike was generated in an oblique branch with input resistance of 810 MΩ. The former NMDA spike recovered after GABAergic inhibition at Δt = 10 ms, whereas the latter NMDA spike terminated for the same inhibition, suggesting that the NMDA spikes in branches with larger input resistance are longer-lasting and more resilient to inhibition (Figure 4B). We computed the Pearson correlation coefficient between various passive properties of the branch and the critical $GABA_A$ conductance required to terminate the NMDA spike (Figure 4C). This critical $GABA_A$ conductance was strongly correlated with the input conductance of the dendritic branch; the smaller the input conductance, the larger the $GABA_A$ conductance required to terminate the NMDA spike. The critical $GABA_A$ conductance was also weakly correlated with the distance of the dendritic branch from the soma (Figure 4C). These results imply that NMDA spike-based plasticity is more likely to take place at distal branches with large input resistance. This result is explained in Figure S3A and the related text.

NMDA Spikes Generated in Multiple Spines: Effects of Dendritic versus Spine Inhibition

Recent work has shown that the effect of synaptic inhibition is highly localized when it impinges on a dendritic spine together with an excitatory synapse located on the same spine (Chiu et al., 2013; Higley, 2014). How would spine inhibition interact with the NMDA spike when generated by a clustered group of excitatory spine synapses when compared to dendritic inhibition? Figures 5A–5C show shows that when placed on the dendritic branch (as is typically the case), timed inhibition could terminate the NMDA spike at all activated spines (Δt = 30 ms, red trace in Figure 5B). When the same inhibitory synapse was placed at the spine head (Figure 5D), in the case of both high spine neck and dendritic input resistance (∼0.8 and ∼1.9GΩ, respectively), the NMDA spike was not terminated at any of the activated spines for time delays ≤ 35 ms (Figure 5E). This was true despite the observation that inhibition on the spine head hyperpolarized that spine voltage more than inhibition on the dendrite. In other words, the cooperative NMDA spike, generated collaboratively at all 20 activated spines, protected the NMDA spikes at individual spines from local inhibitory input. Furthermore, the concentration of Ca^{2+} flowing into the spine head through the NMDA receptors maximally dropped by ∼40% when inhibition impinged on the dendrite (Figure 5C) but only by 30% when the inhibition was located on the spine head (Figure 5F). The vulnerability function for both the NMDA voltage time integral (Figure 5G) and the time integral of the total Ca^{2+} concentration entering through the NMDA channels (Figure 5H) demonstrate the increased effect of dendritic versus spine inhibition. This has important implications for branch-specific plasticity processes as elaborated on in the Discussion.

As shown in Figure S4, for spines with large neck resistance, the local inhibitory shunt at the spine head membrane does not propagate well to the adjacent spines. This implies that the collective NMDA current generated by the adjacent dendritic spines is only weakly affected by inhibition on a single spine. However, this collective NMDA-mediated current does effectively flow from the dendrite into the spine head membrane (in this case the spine base and the spine head are essentially isopotential) (Segev and Rall, 1988). In contrast, when inhibition is located directly on the stem dendrite, it shunts more effectively the spine head membrane (A. Gidon and I. Segev, unpublished data), and it also electrically decouples the spines from each other, thus dampening more powerfully the depolarization in each of the activated spines.

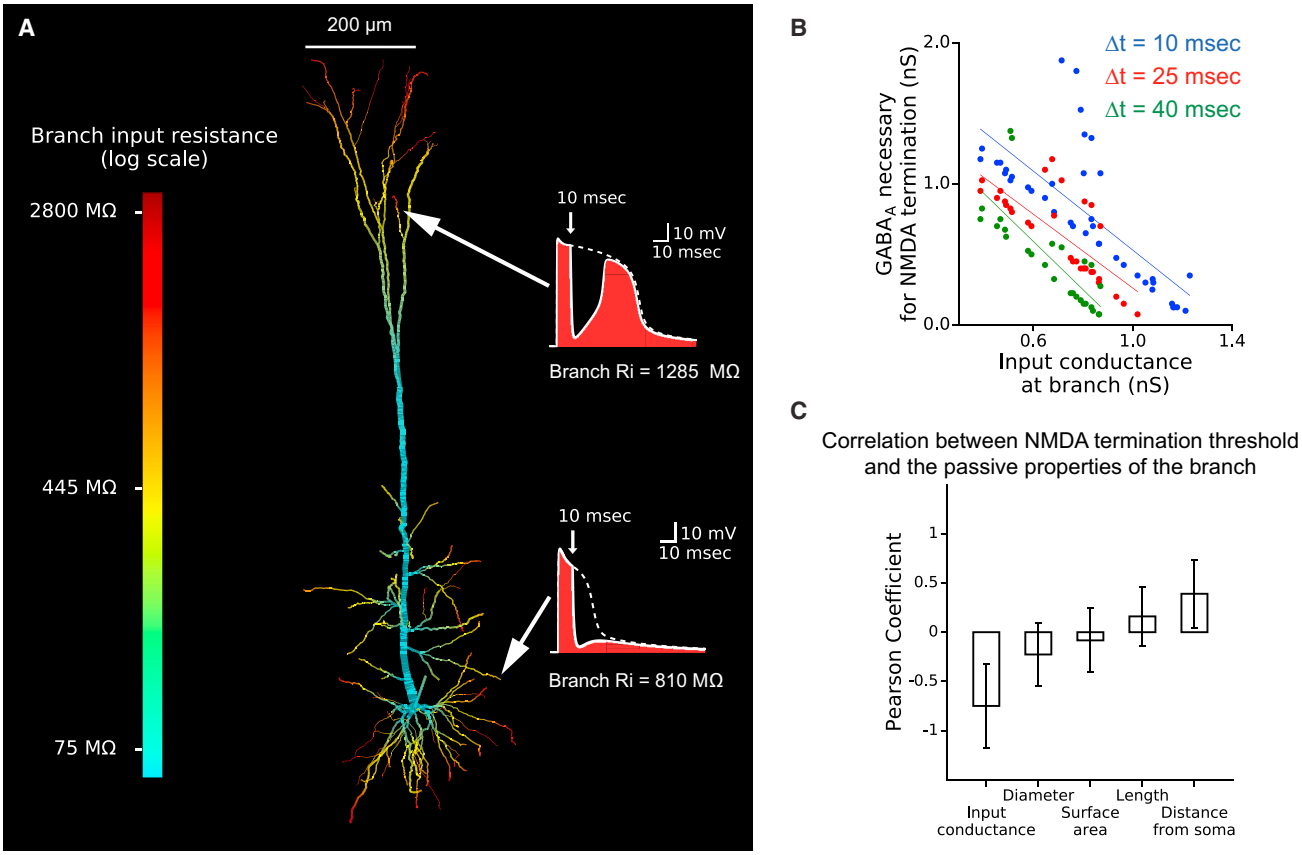

Figure 4. NMDA Spikes Are Resilient to Inhibition in Dendritic Branches with Large Input Resistance

(A) NMDA spike with time inhibition in dendritic branches with large input resistance (top right) and with a smaller input resistance (bottom right). NMDA spikes in control conditions (dashed line). White arrows point to the activated branches. Dendritic branches are colored by their input resistance (log scale on left).

(B) The critical $GABA_A$ conductance required to terminate an NMDA spike as a function of branch input conductance. Three cases of inhibition arriving at different delays with respect to excitation are shown.

(C) Correlation between the critical $GABA_A$ conductance and various properties of the dendritic branches, averaged over inhibition activation times. Note that the input conductance of the branch was strongly correlated with the critical $GABA_A$ conductance. Bars indicate the mean Pearson correlation over all tested $GABA_A$ conductances; error bars indicate the SD.

Fine-Tuned Modulation of the Neuron's Output by Timed Inhibition Interacting with Dendritic NMDA Spikes

Next, we utilized the full nonlinear model of the L5 pyramidal cell used above to examine how branch-specific timed inhibition interacting with local NMDA spikes controls the output of this cell. Multiple distal dendritic branches were synchronously excited as shown in Figure 6A. Figure 6C shows the fine modulation of the somatic Na^+ spikes by local dendritic inhibition; without inhibition the neuron fired a burst of 2.5 spikes on average in response to the activated dendritic NMDA spikes (Figure 6B, similar to Milojkovic et al., 2004; Polsky et al., 2009). When inhibition was activated at $\Delta t = 0$ ms, only two Na^+ spikes were generated at the modeled axon, with a further decrease to one spike when $\Delta t = 10$ ms and no output spikes with $\Delta t = 20$ ms (Figure 6C). When averaging over 60 combinations of activated terminal basal dendritic branches, the number of spikes evoked in the soma as a function of Δt (Figure 6D) resembled the vulnerability function of a single NMDA spike in a single branch (Figure 1C). As a whole, Figure 6 demonstrates that sparse and weak inhibition in distal dendritic branches was able to strongly modulate the neuron's output when it was well timed during the plateau phase of local dendritic NMDA spikes.

DISCUSSION

Our dynamic system analysis and computational study suggests that due to its unique dynamics, the NMDA spike is sensitive to well-timed and strategically located dendritic inhibition. Inhibition located at the dendritic site of the NMDA spike generation, or a few tens of micrometers distal to it, was able to finely and powerfully tune the time course of the NMDA spike and its corresponding current influx (Figures 1 and 2). There are two distinct regimes for the effect of synaptic inhibition on the NMDA spike. In its early phase, weak synaptic inhibition transiently hyperpolarized the NMDA spike; it then fully recovered back to its original trajectory. At later arrival times, inhibition prematurely terminated the NMDA spike (Figure 1C). This vulnerability of the NMDA spike to inhibition holds for inhibition

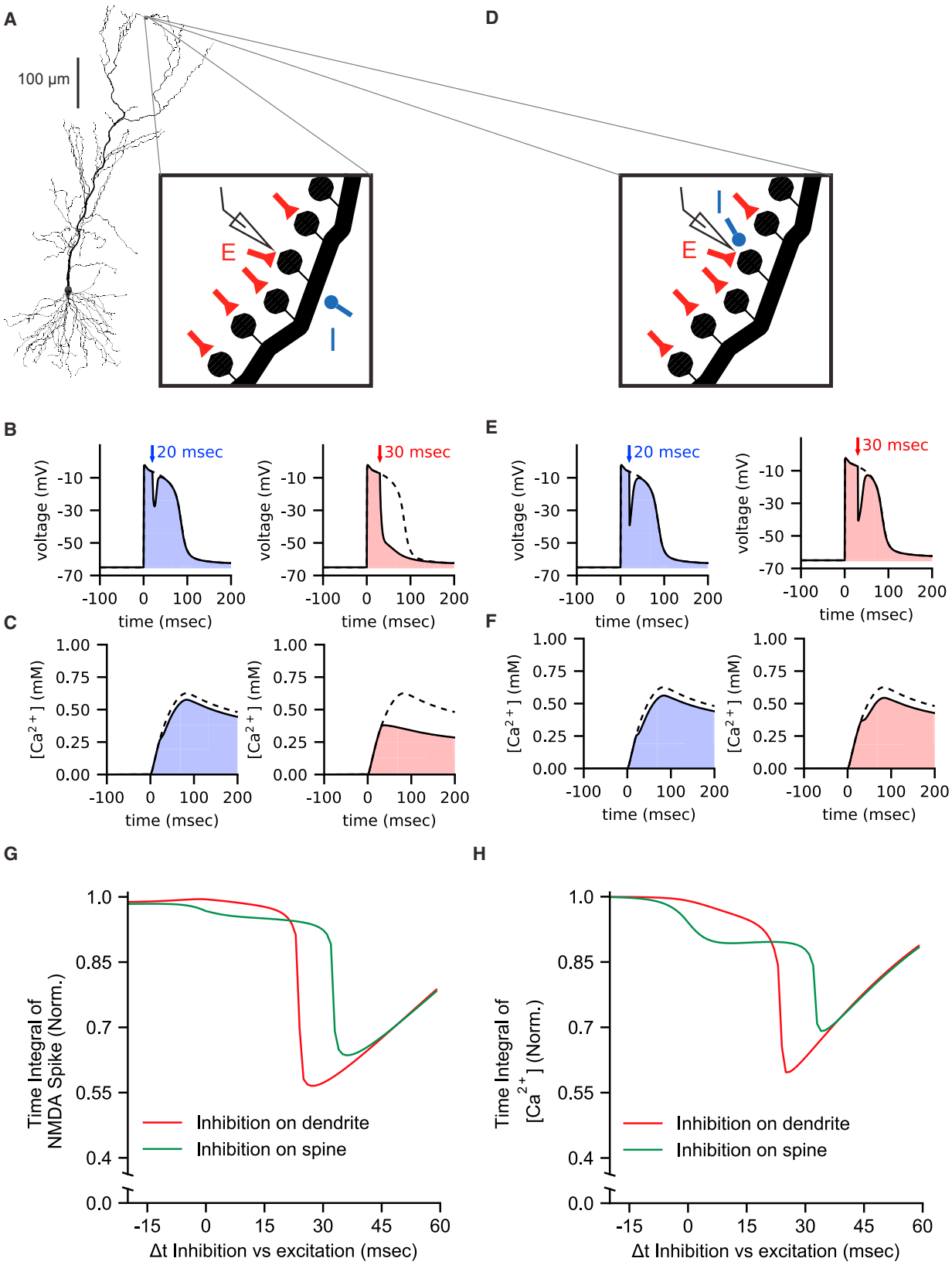

(legend on next page)

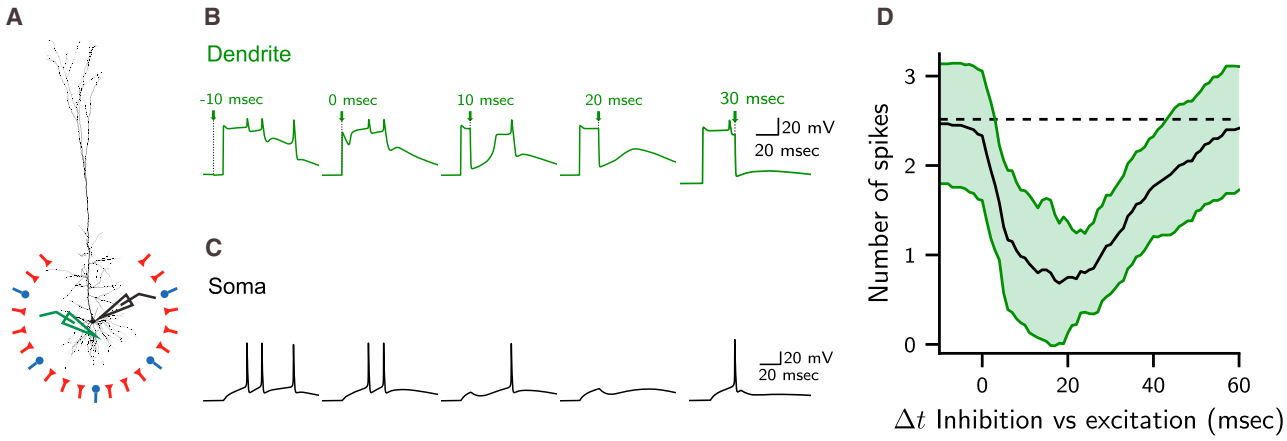

Figure 6. Interaction of Timed Dendritic Inhibition with Dendritic NMDA Spikes Finely Modulates the Neuron's Output

(A) Sixteen basal dendritic terminals synchronously activated, each by 20 excitatory and 2 inhibitory synapses. Voltage was recorded from the soma (black electrode) and from one of the activated branches (green electrode).

(B) Local NMDA spike modulated by local timed inhibition. Arrows indicate the timing of inhibition with respect to excitation. Voltage was recorded from the green electrode in (A).

(C) Somatic spikes for the respective cases shown in (B).

(D) Mean (black line) and standard deviation (green lines) of 60 possible combinations of 16 activated terminal basal branches as in (C). The dashed line is the average number of spikes in the control condition without inhibition.

both impinging on the location of the excitatory synapses and distal to the spike, but the inhibitory effect diminishes steeply for more proximal synapses, making the effect of inhibition on the NMDA spike a branch-specific phenomenon (Figure 2). Depending on the time of inhibition with respect to excitation, inhibition may gradually reduce the NMDA-related Ca^{2+} influx by up to 40% (Figure 5C). Dynamical systems theory enabled us to explain the vulnerability of the NMDA spike to timed inhibition (Figure 3).

We also explored and mechanistically explained the finding that, within a certain time-window, synaptic inhibition increases, rather than decreases, the inward NMDA current (Figure S2) and characterizes the shift of the NMDA spike duration over the different dendritic branches from a unimodal to bimodal distribution when a distributed dendritic inhibition is activated (Figure S6). Next, we showed that stronger and longer-lasting NMDA spikes (in distal dendrites with large input resistance) persist in the face of local inhibition, whereas weaker NMDA spikes (on proximal branches with smaller input resistance) are more susceptible to inhibition (Figures 4 and S3). By simulating the case of an NMDA spike generated cooperatively in the head membrane of a group of dendritic spines we showed that timed inhibition impinging directly on the dendrite effectively controls the NMDA spike in all spines involved, but that the same NMDA spike was more resilient to local inhibition impinging on individual dendritic spines (Figure 5). Finally, we demonstrated that weak inhibition impinging on several distal basal dendrites could finely modulate the branch-specific NMDA spikes and, consequently, the number of output Na^{+} spikes in the soma (Figure 6). This finding is consistent with the recent *in vitro* and *in vivo* findings (Lovett-Barron et al., 2012; Royer et al., 2012).

Dendritic Inhibition and NMDA-Induced Plasticity

NMDA spikes are known to be involved in facilitating long-term potentiation (LTP) and long-term depression (LTD) (Brandalise et al., 2016; Gambino et al., 2014; Golding et al., 2002; Gordon et al., 2006; Sandler et al., 2016). We showed that timed local

Figure 5. The NMDA Spike and Its Corresponding Ca^{2+} Influx Are Strongly Affected by Dendritic Inhibition and Are Less Affected by Spine Inhibition

(A) CA1 pyramidal cell model with dendritic spines on the most distal 20 μm of a distal apical branch; each spine head contained AMPA- and NMDA-based excitatory synapses (red). A single $GABA_A$ synapse (blue) was placed on the dendrite in the center of the modeled spines. Schematic electrode shows recording location of voltage and Ca^{2+} concentration.

(B) NMDA spikes generated by activating 20 spinous excitatory synapses synchronously in the branch shown in (A). The inhibitory synapse was activated at either Δt = 20 ms (blue) or 30 ms (red).

(C) As in (B) for the total [Ca^{2+}] in the spine head.

(D) As in (A), with inhibition impinging on the spine head.

(E) As in (B), with inhibition impinging on the spine head.

(F) As in (C), with inhibition impinging on the spine head.

(G) Vulnerability function of the NMDA spike in the spine head when inhibition impinges at the spine head (green, as in D) or at the dendrite (red, as in A).

(H) As in (G), but for total calcium concentration [Ca^{2+}]. In all cases, the spine neck resistance was 820 MΩ. The only source of Ca^{2+} in the model was NMDA channels.

inhibition could gradually reduce the NMDA-dependent current influx by up to 40% in a group of spines cooperatively involved in generating the NMDA spike (Figure 5). Considering the Ca^{2+} control theory for inducing plasticity (Graupner and Brunel, 2012; Shouval et al., 2002; see also Bar-Ilan et al., 2013), this finding implies that weak local dendritic inhibition powerfully controls plasticity in a specific group of spatially clustered dendritic spines. This expands upon previous studies showing the impact of inhibition on plasticity induced by the back-propagating action potential and by dendritic Ca^{2+} spikes (Müllner et al., 2015; Pérez-Garci et al., 2013; Wilmes et al., 2016). Another effect that timed dendritic inhibition might have on dendritic plasticity is the suppression of the briefer NMDA spikes in terminal branches with relatively low input resistance, keeping intact the longer-lasting NMDA spikes in dendritic terminals with large input resistance (Figure 4). Consequently, timed dendritic inhibition could act as a cellular mechanism protecting the neuron from the influence of shorter NMDA spikes that, perhaps, carry less information relevant to its overall computation, while leaving intact the longer, more resilient NMDA spikes (Figure S3).

Fine-Tuning of the Neuron's Output by Sparse Inhibition Interacting with NMDA Spikes: Implications for High-Level Functions

The NMDA spike, even when occurring on a distal apical dendritic branch, significantly boosts the excitatory charge reaching the soma. Several such dendritic spikes could generate a burst of output spikes in the axon (Milojkovic et al., 2004; Polsky et al., 2009). In the present study we showed that the number of spikes in this output burst could be finely modulated by weak spatially distributed dendritic inhibition targeting specific dendritic branches that generate local NMDA spike. Recently, Iacaruso et al. (2017) and Wilson et al. (2016) showed that in V1, the receptive fields of cortical neurons are strongly shaped by local nonlinear dendritic responses resulting from spatially clustered excitatory synaptic input. In this case, branch-specific synaptic inhibition could very effectively modulate the functional/computational properties of the neuron (e.g., by shifting its receptive field and modulating top-down and bottom-up interactions) (see Palmer et al., 2014) and, consequently, the high-level function of the whole system that they are part of. Another study led to the hypothesis that temporal windows for computation and integration of inputs are determined by oscillations of interneuron activity (e.g., Mizuseki et al., 2009). Our study may shed light on how temporally precise inhibition may confine such computational windows. We thus suggest an additional perspective to the growing number of studies highlighting the computational advantages of branch-specific dendritic nonlinearity at both cellular and system levels.

Robustness of the Results and Comparisons with Other Studies

In this work we primarily used the Jahr and Stevens model for the NMDA current (see the Experimental Procedures) as do many contemporary theoretical studies. However, some experimental work (Clarke and Johnson, 2008; Kampa et al., 2004; Moradi et al., 2013; Vargas-Caballero and Robinson, 2004) has led to a new and potentially more realistic model of the NMDA current. We therefore confirmed our key results using alternative models for the NMDA spike (Figure S1), in particular its biphasic vulnerability function. The magnitude of the effect of timed inhibition and its exact timing with respect to the NMDA plateau phase was sensitive to the specific model used. We also examined our key results under *in vivo*-like conditions wherein the membrane is expected to be more depolarized and shunted (Figures S5A and S5B) because of background synaptic activity (Rapp et al., 1992), and inhibitory inputs are likely to arrive with some temporal jitter (Figures S5C and S5D). The biphasic nature of the vulnerability function of the NMDA spike to inhibition remained, although it was stronger at the shunted case and weaker with additional jitter.

Notably, Rhodes (2006) was the first to study the effect of timed inhibition on the NMDA spike. In his study, the NMDA/AMPA conductance ratio was much larger than in our study (10:1 and 1:1, respectively) and the inhibitory conductance in his work was larger. Consequently, the Rhodes study demonstrated the termination phase but did not show the two-phase effect of inhibition on the NMDA spike (Figures 1 and 3), nor did it explore the gradual effect of inhibition over the NMDA-related current influx or its effect on the output spikes. Another study (Jadi et al., 2012) has considered the effect of inhibition preceding the NMDA spike or when activated during its onset, but they did not explore the impact of inhibition during the plateau phase of the NMDA spike as studied here.

Experimental Predictions and Extension of This Work

The key prediction of this study is that the NMDA spike dynamics exhibit biphasic vulnerability to timed inhibition. This prediction could be examined experimentally in a variety of experiments, by activating a local NMDA spike *in vitro* (e.g., by glutamate uncaging) and hyperpolarizing the membrane by either $GABA_A$ uncaging (e.g., Kantevari et al., 2010) or by brief hyperpolarizing somatic voltage-clamp or current-clamp at different times relative to the NMDA spike initiation. Importantly, an *in vitro* experimental work in the mouse striatum was recently published, validating our theoretical predictions concerning the fine modulation of the NMDA-spike by weak and precisely timed synaptic inhibition in that area (Du et al., 2017). Our study predicts that, at the soma, the resultant voltage will show the biphasic behavior of the NMDA spike with timed inhibition. Similar experiments (combining glutamate and $GABA_A$ uncaging) could be performed to examine the prediction (Figure 6) that the number of spikes in the NMDA-induced somatic burst could be modulated by sparse dendritic inhibition. Using dendritic Ca^{2+} imaging during the NMDA spike, our prediction of a large simultaneous Ca^{2+} influx in a cluster of dendritic spines as well as the strong impact of dendritic inhibition on the Ca^{2+} dynamics could be examined experimentally (Figure 5).

Finally, our study could be extended in various directions. We did not include in the dynamical system analysis (Figure 3) other voltage-dependent ion channels that might shape the NMDA spike (e.g., voltage-dependent K^+ and Na^+ currents). We also simplified our analytical exploration using an isopotential neuron; although difficult, this analysis should be extended to an NMDA spike generated in an electrically distributed system. It will also be interesting to model the impact of timed inhibition on other

dendritic spikes (e.g., dendritic Ca^{2+} spike). These and other expansions will have to wait for the near future.

EXPERIMENTAL PROCEDURES

NEURON Models and Simulations

The models and simulations were carried out in the NEURON simulator, wrapped with a python script (Carnevale and Hines, 2006). All models can be found in ModelDB, with scripts to recreate the figures (Database: http://modeldb.yale.edu/231427). We chose to use several models to characterize the effect of timed inhibition on the NMDA spike. The full nonlinear L5 pyramidal model (Hay et al., 2011) was used in Figures 6, S5A, S5B, and S6. The corresponding passive model was used in Figures 1, 2, 4, S1, S5C, S5D, and S7, with a resting potential of −80 mV. We used an isopotential passive model in combination with the dynamic system theory to analyze the impact of timed inhibition on the NMDA current (Figures 3, S2, and S3). The isopotential model consisted of a soma 20 μm in diameter, with an R_m of 20,000 Ωcm^2, C_m of 1 $\mu F/cm^2$, and a resting potential of −80 mV. For spine-head inhibition in Figure 5, we used the CA1 pyramidal cell model of Grunditz et al. (2008).

Excitatory synapses were placed on distal apical branches (Figures 1, 2, 4, and S6) or distal basal branches (Figures 4, 6, and S6), with 1 excitatory synapse per 2.2 μm on the middle 44 μm of the branch (for Figures 1 and 2), every 1 μm on the last 20 μm of the branch (for Figures 4, 6, and S6), or every 1 μm on the 7 to 27 μm of the branch (Figure S7). Inhibitory synapses were spatially located in the center of the excitatory synapses, except in Figure 2, where inhibition was located either in the center, 35 μm more distal or 35 μm more proximal to it.

Synaptic Models

We used the model of Jahr and Stevens (1990) for the NMDA current, with the gamma parameter shifted from 0.062 to 0.08 (Poleg-Polsky, 2015; Rhodes, 2006). $GABA_A$ and AMPA conductance were modeled as double exponents, with the $GABA_A$ rise and decay times being 0.18 and 5 ms, respectively (Salin and Prince, 1996), and 0.2 and 1.7 ms, respectively, for the AMPA conductance (Spruston et al., 1995). The NMDA rise and decay times were 2 and 75 ms, respectively (Rhodes, 2006). The $GABA_A$ reversal potential was −80 and 0 mV for the NMDA and AMPA receptors. The NMDA-to-AMPA ratio was 1:1 (Hay et al., 2011).

Excitatory and Inhibitory Interaction

We activated the excitatory synapses simultaneously to generate a dendritic NMDA spike. The $GABA_A$ synapses were activated at different Δt with respect to the excitatory synapses ranging from 20 ms before excitation to 60 ms after excitation with 1-ms steps (Figures 1, 2, 6, S1, S2, S4, and S6). Voltage was recorded from the center of the synapse distribution on the branch in the morphological model. The NMDA current was the sum of current generated by all excitatory synapses. For the calculation of the normalized voltage integrals, we summed the voltage after adding the resting potential to have a positive-sign result and then divided by the voltage integral of the control case. For the calculation of the normalized current integrals, we summed the current and then divided by the current integral of the control case.

Momentary V-I Curves

Momentary V-I curves (Figures 3 and S3) were calculated by running the simulations up to a given time point, then clamping the membrane voltage between −90 and 0 mV, with 0.1 mV steps, and recording the currents 1 ms following the voltage clamp. Because the membrane time constant is faster than the decay time constant of the NMDA current, we considered the voltage as instantaneous with respect to the current. To create the trajectory of the fixed points over time (Figure 3B), we recorded the intersections of NMDA and leak currents. The voltage trace in these figures was created using the same excitatory and inhibitory conductances and activation times without voltage clamp. In all V-I curve calculations, the peak NMDA conductance was 7.5 nS, and peak $GABA_A$ conductance was 1.5 nS.

Simultaneous Activation of Several Dendritic Branches

In Figure 6, 20 AMPA/NMDA synapses (0.4 nS peak each) were activated on each of the 16 different basal dendritic terminal branches. Synapses were uniformly distributed on the most distal 20 μm of each dendrite. In each branch, two inhibitory synapses (1 nS each) were placed in the center of the excitatory synapses. For Figure 6D, 60 possible combinations of the 16 unique different basal dendritic terminal branches were randomly selected.

Termination Threshold for the NMDA Spike

To calculate the $GABA_A$ conductance required to terminate the NMDA spike (Figures 4 and S3), we varied the peak of GABA conductances between 0.05 nS and 2.15 nS, with steps of 0.025 nS, and calculated the derivative of the integral of the membrane voltage with respect to each conductance. The peak $GABA_A$ conductance that resulted with the minimal derivative was defined as the conductance threshold for terminating the NMDA spike. In cases in which such a termination threshold was not calculated (Figures 1, 2, 3, 5, and 6), we defined "premature termination" when the half-width of the NMDA spike was smaller than 90% of the control case.

$[Ca^{2+}]$ Concentration and Voltage Recording in the Spine Head

In Figure 5, we used the CA1 pyramidal cell model, including models of dendritic spines, like in (Grunditz et al., 2008). We removed the R-type calcium channels from that model to focus on the effect of spine morphology on the interaction between timed inhibition and excitation.

SUPPLEMENTAL INFORMATION

Supplemental Information includes Supplemental Experimental Procedures and seven figures and can be found with this article online at https://doi.org/10.1016/j.celrep.2017.10.035.

AUTHOR CONTRIBUTIONS

M.D. and I.S. conceived the study and wrote the manuscript. M.D. carried out the analysis. G.C., E.M., and H.M. participated in several key discussions related to this study.

ACKNOWLEDGMENTS

This work was supported by the Gatsby Charitable Foundation and the EPFL-Hebrew University Collaborative Grant, the EPFL support to the Laboratory of Neural Microcircuitry (LNMC), the ETH Domain for the Blue Brain Project (BBP), and the Human Brain Project (HBP) from the European Union Seventh Framework Program (FP7/2007-2013) (grant 604102).

Received: May 25, 2017
Revised: August 17, 2017
Accepted: October 8, 2017
Published: November 7, 2017

REFERENCES

Bar-Ilan, L., Gidon, A., and Segev, I. (2013). The role of dendritic inhibition in shaping the plasticity of excitatory synapses. Front. Neural Circuits *6*, 118.

Branco, T., and Häusser, M. (2011). Synaptic integration gradients in single cortical pyramidal cell dendrites. Neuron *69*, 885–892.

Branco, T., Clark, B.A., and Häusser, M. (2011). Dendritic discrimination of temporal input sequences in cortical neurons. Science *329*, 1671–1676.

Brandalise, F., Carta, S., Helmchen, F., Lisman, J., and Gerber, U. (2016). Dendritic NMDA spikes are necessary for timing-dependent associative LTP in CA3 pyramidal cells. Nat. Commun. *7*, 13480.

Carnevale, N.T., and Hines, M.L. (2006). The NEURON Book (Cambridge University Press).

Chiu, C.Q., Lur, G., Morse, T.M., Carnevale, N.T., Ellis-Davies, G.C.R., and Higley, M.J. (2013). Compartmentalization of GABAergic inhibition by dendritic spines. Science *340*, 759–762.

Clarke, R.J., and Johnson, J.W. (2008). Voltage-dependent gating of NR1/2B NMDA receptors. J. Physiol. *586*, 5727–5741.

Cuntz, H., Remme, M.W.H., and Torben-Nielsen, B. (2014). The Computing Dendrite (Springer).

Du, K., Wu, Y.-W., Lindroos, R., Liu, Y., Rózsa, B., Katona, G., Ding, J.B., and Kotaleski, J.H. (2017). Cell-type-specific inhibition of the dendritic plateau potential in striatal spiny projection neurons. Proc. Natl. Acad. Sci *114*, E7612–7621.

Gambino, F., Pagès, S., Kehayas, V., Baptista, D., Tatti, R., Carleton, A., and Holtmaat, A. (2014). Sensory-evoked LTP driven by dendritic plateau potentials in vivo. Nature *515*, 116–119.

Gidon, A., and Segev, I. (2012). Principles governing the operation of synaptic inhibition in dendrites. Neuron *75*, 330–341.

Golding, N.L., Staff, N.P., and Spruston, N. (2002). Dendritic spikes as a mechanism for cooperative long-term potentiation. Nature *418*, 326–331.

Gordon, U., Polsky, A., and Schiller, J. (2006). Plasticity compartments in basal dendrites of neocortical pyramidal neurons. J. Neurosci. *26*, 12717–12726.

Graupner, M., and Brunel, N. (2012). Calcium-based plasticity model explains sensitivity of synaptic changes to spike pattern, rate, and dendritic location. Proc. Natl. Acad. Sci. USA *109*, 3991–3996.

Grunditz, A., Holbro, N., Tian, L., Zuo, Y., and Oertner, T.G. (2008). Spine neck plasticity controls postsynaptic calcium signals through electrical compartmentalization. J. Neurosci. *28*, 13457–13466.

Hay, E., Hill, S., Schürmann, F., Markram, H., and Segev, I. (2011). Models of neocortical layer 5b pyramidal cells capturing a wide range of dendritic and perisomatic active properties. PLoS Comput. Biol. *7*, e1002107.

Higley, M.J. (2014). Localized GABAergic inhibition of dendritic Ca(2+) signalling. Nat. Rev. Neurosci. *15*, 567–572.

Hoffman, D.A., Magee, J.C., Colbert, C.M., and Johnston, D. (1997). K+ channel regulation of signal propagation in dendrites of hippocampal pyramidal neurons. Nature *387*, 869–875.

Iacaruso, M.F., Gasler, I.T., and Hofer, S.B. (2017). Synaptic organization of visual space in primary visual cortex. Nature *547*, 449–452.

Jack, J.J.B., Noble, D., and Tsien, R.W. (1975). Electric Current Flow in Excitable Cells (Clarendon Press).

Jadi, M., Polsky, A., Schiller, J., and Mel, B.W. (2012). Location-dependent effects of inhibition on local spiking in pyramidal neuron dendrites. PLoS Comput. Biol. *8*, e1002550.

Jahr, C.E., and Stevens, C.F. (1990). Voltage dependence of NMDA-activated macroscopic conductances predicted by single-channel kinetics. J. Neurosci. *10*, 3178–3182.

Johnston, D., and Narayanan, R. (2008). Active dendrites: colorful wings of the mysterious butterflies. Trends Neurosci. *31*, 309–316.

Kampa, B.M., Clements, J., Jonas, P., and Stuart, G.J. (2004). Kinetics of Mg2+ unblock of NMDA receptors: implications for spike-timing dependent synaptic plasticity. J. Physiol. *556*, 337–345.

Kantevari, S., Matsuzaki, M., Kanemoto, Y., Kasai, H., and Ellis-Davies, G.C.R. (2010). Two-color, two-photon uncaging of glutamate and GABA. Nat. Methods *7*, 123–125.

Klausberger, T. (2009). GABAergic interneurons targeting dendrites of pyramidal cells in the CA1 area of the hippocampus. Eur. J. Neurosci. *30*, 947–957.

Larkum, M.E., and Nevian, T. (2008). Synaptic clustering by dendritic signalling mechanisms. Curr. Opin. Neurobiol. *18*, 321–331.

Larkum, M.E., Zhu, J.J., and Sakmann, B. (1999). A new cellular mechanism for coupling inputs arriving at different cortical layers. Nature *398*, 338–341.

Lavzin, M., Rapoport, S., Polsky, A., Garion, L., and Schiller, J. (2012). Nonlinear dendritic processing determines angular tuning of barrel cortex neurons in vivo. Nature *490*, 397–401.

Lovett-Barron, M., Turi, G.F., Kaifosh, P., Lee, P.H., Bolze, F., Sun, X.-H., Nicoud, J.-F., Zemelman, B.V., Sternson, S.M., and Losonczy, A. (2012). Regulation of neuronal input transformations by tunable dendritic inhibition. Nat. Neurosci. *15*, 423–430, S1–S3.

Ma, W.P., Liu, B.H., Li, Y.T., Huang, Z.J., Zhang, L.I., and Tao, H.W. (2010). Visual representations by cortical somatostatin inhibitory neurons–selective but with weak and delayed responses. J. Neurosci. *30*, 14371–14379.

Magee, J.C. (2016). Dendritic voltage-gated ion channels. In Dendrites, G. Stuart, N. Spruston, and M. Häusser, eds. (Oxford University Press), pp. 259–284.

Major, G., Polsky, A., Denk, W., Schiller, J., and Tank, D.W. (2008). Spatiotemporally graded NMDA spike/plateau potentials in basal dendrites of neocortical pyramidal neurons. J. Neurophysiol. *99*, 2584–2601.

Major, G., Larkum, M.E., and Schiller, J. (2013). Active properties of neocortical pyramidal neuron dendrites. Annu. Rev. Neurosci. *36*, 1–24.

Markram, H., Toledo-Rodriguez, M., Wang, Y., Gupta, A., Silberberg, G., and Wu, C. (2004). Interneurons of the neocortical inhibitory system. Nat. Rev. Neurosci. *5*, 793–807.

Mel, B.W. (1992). NMDA-based pattern discrimination in a modeled cortical neuron. Neural Comput. *4*, 502–517.

Mel, B.W. (1993). Synaptic integration in an excitable dendritic tree. J. Neurophysiol. *70*, 1086–1101.

Milojkovic, B.A., Radojicic, M.S., Goldman-Rakic, P.S., and Antic, S.D. (2004). Burst generation in rat pyramidal neurones by regenerative potentials elicited in a restricted part of the basilar dendritic tree. J. Physiol. *558*, 193–211.

Mizuseki, K., Sirota, A., Pastalkova, E., and Buzsáki, G. (2009). Theta oscillations provide temporal windows for local circuit computation in the entorhinal-hippocampal loop. Neuron *64*, 267–280.

Moradi, K., Moradi, K., Ganjkhani, M., Hajihasani, M., Gharibzadeh, S., and Kaka, G. (2013). A fast model of voltage-dependent NMDA receptors. J. Comput. Neurosci. *34*, 521–531.

Müllner, F.E., Wierenga, C.J., and Bonhoeffer, T. (2015). Precision of inhibition: dendritic inhibition by individual GABAergic synapses on hippocampal pyramidal cells is confined in space and time. Neuron *87*, 576–589.

Nevian, T., Larkum, M.E., Polsky, A., and Schiller, J. (2007). Properties of basal dendrites of layer 5 pyramidal neurons: a direct patch-clamp recording study. Nat. Neurosci. *10*, 206–214.

Palmer, L.M., Shai, A.S., Reeve, J.E., Anderson, H.L., Paulsen, O., and Larkum, M.E. (2014). NMDA spikes enhance action potential generation during sensory input. Nat. Neurosci. *17*, 383–390.

Pérez-Garci, E., Larkum, M.E., and Nevian, T. (2013). Inhibition of dendritic Ca2+ spikes by GABAB receptors in cortical pyramidal neurons is mediated by a direct Gi/o-β-subunit interaction with Cav1 channels. J. Physiol. *591*, 1599–1612.

Poirazi, P., and Mel, B.W. (2001). Impact of active dendrites and structural plasticity on the memory capacity of neural tissue. Neuron *29*, 779–796.

Poirazi, P., Brannon, T., and Mel, B.W. (2003a). Pyramidal neuron as two-layer neural network. Neuron *37*, 989–999.

Poirazi, P., Brannon, T., and Mel, B.W. (2003b). Arithmetic of subthreshold synaptic summation in a model CA1 pyramidal cell. Neuron *37*, 977–987.

Poleg-Polsky, A. (2015). Effects of neural morphology and input distribution on synaptic processing by global and focal NMDA-spikes. PLoS ONE *10*, e0140254.

Polsky, A., Mel, B., and Schiller, J. (2009). Encoding and decoding bursts by NMDA spikes in basal dendrites of layer 5 pyramidal neurons. J. Neurosci. *29*, 11891–11903.

Pouille, F., and Scanziani, M. (2001). Enforcement of temporal fidelity in pyramidal cells by somatic feed-forward inhibition. Science *293*, 1159–1163.

Rall, W., and Shepherd, G.M. (1968). Theoretical reconstruction of field potentials and dendrodendritic synaptic interactions in olfactory bulb. J. Neurophysiol. *6*, 884–915.

Rall, W., Shepherd, G.M., Reese, T.S., and Brightman, M.W. (1966). Dendrodendritic synaptic pathway for inhibition in the olfactory bulb. Exp. Neurol. *14*, 44–56.

Rapp, M., Yarom, Y., and Segev, I. (1992). The impact of parallel fiber background activity on the cable properties of cerebellar Purkinje cells. Neural Comput. *4*, 518–533.

Rhodes, P. (2006). The properties and implications of NMDA spikes in neocortical pyramidal cells. J. Neurosci. *26*, 6704–6715.

Royer, S., Zemelman, B.V., Losonczy, A., Kim, J., Chance, F., Magee, J.C., and Buzsáki, G. (2012). Control of timing, rate and bursts of hippocampal place cells by dendritic and somatic inhibition. Nat. Neurosci. *15*, 769–775.

Salin, P.A., and Prince, D.A. (1996). Spontaneous GABAA receptor-mediated inhibitory currents in adult rat somatosensory cortex. J. Neurophysiol. *75*, 1573–1588.

Sanders, H., Berends, M., Major, G., Goldman, M.S., and Lisman, J.E. (2013). NMDA and GABAB (KIR) conductances: the "perfect couple" for bistability. J. Neurosci. *33*, 424–429.

Sandler, M., Shulman, Y., and Schiller, J. (2016). A novel form of local plasticity in tuft dendrites of neocortical somatosensory layer 5 pyramidal neurons. Neuron *90*, 1028–1042.

Schiller, J., and Schiller, Y. (2001). NMDA receptor-mediated dendritic spikes and coincident signal amplification. Curr. Opin. Neurobiol. *11*, 343–348.

Schiller, J., Major, G., Koester, H.J., and Schiller, Y. (2000). NMDA spikes in basal dendrites of cortical pyramidal neurons. Nature *404*, 285–289.

Segev, I., and Rall, W. (1988). Computational study of an excitable dendritic spine. J. Neurophysiol. *60*, 499–523.

Shouval, H.Z., Bear, M.F., and Cooper, L.N. (2002). A unified model of NMDA receptor-dependent bidirectional synaptic plasticity. Proc. Natl. Acad. Sci. USA *99*, 10831–10836.

Silberberg, G., and Markram, H. (2007). Disynaptic inhibition between neocortical pyramidal cells mediated by Martinotti cells. Neuron *53*, 735–746.

Smith, S.L., Smith, I.T., Branco, T., and Häusser, M. (2013). Dendritic spikes enhance stimulus selectivity in cortical neurons in vivo. Nature *503*, 115–120.

Spruston, N., Jonas, P., and Sakmann, B. (1995). Dendritic glutamate receptor channels in rat hippocampal CA3 and CA1 pyramidal neurons. J. Physiol. *482* (*Pt 2*), 325–352.

Stokes, C.C., Teeter, C.M., and Isaacson, J.S. (2014). Single dendrite-targeting interneurons generate branch-specific inhibition. Front. Neural Circuits *8*, 139.

Vargas-Caballero, M., and Robinson, H.P. (2004). Fast and slow voltage-dependent dynamics of magnesium block in the NMDA receptor: the asymmetric trapping block model. J. Neurosci. *24*, 6171–6180.

Villa, K.L., Berry, K.P., Subramanian, J., Cha, J.W., Oh, W.C., Kwon, H.-B., Kubota, Y., So, P.T.C., and Nedivi, E. (2016). Inhibitory synapses are repeatedly assembled and removed at persistent sites in vivo. Neuron *89*, 756–769.

Wehr, M., and Zador, A.M. (2003). Balanced inhibition underlies tuning and sharpens spike timing in auditory cortex. Nature *426*, 442–446.

Wilmes, K.A., Sprekeler, H., and Schreiber, S. (2016). Inhibition as a binary switch for excitatory plasticity in pyramidal neurons. PLoS Comput. Biol. *12*, e1004768.

Wilson, D.E., Whitney, D.E., Scholl, B., and Fitzpatrick, D. (2016). Orientation selectivity and the functional clustering of synaptic inputs in primary visual cortex. Nat. Neurosci. *19*, 1003–1009.